Solar Energy 274 (2024) 112603

Contents lists available at ScienceDirect

Solar Energy

journal homepage: www.elsevier.com/locate/solener

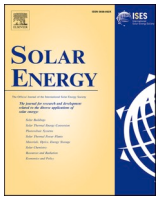

Optical properties enhancement of thermal energy media for consistently high solar absorptivity

Kyu Bum Han [a,*], Eunjin Jeon [a], Patrick Davenport [b], Jason Schirck [c], Michael Adams [d], Shannon Yee [d], Zhiwen Ma [b,*]

[a] Advanced Materials Scientia LLC, 22722 29th Drive Southeast Suite 100, Bothell, WA, 98021, USA
[b] National Renewable Energy Laboratory, 15013 Denver West Parkway, Golden, CO, 80401, USA
[c] Department of Mechanical Engineering, Purdue University, 585 Purdue Mall, West Lafayette, IN, 47907, USA
[d] School of Mechanical Engineering, Georgia Institute of Technology, 801 Ferst Drive Northwest, Atlanta, GA, 30318, USA

ARTICLE INFO

Keywords:
Thermal Energy Media
Concentrating Solar Power
Particle
Low Cost

ABSTRACT

This study aimed to evaluate the optical properties of particles intended for use as thermal energy absorbers in generation 3 concentrated solar power systems. Their characterization involved UV–Vis NIR measurements with an integrating sphere for solar absorptivity, while a reflectometer was employed to measure thermal emittance. By combining absorptivity and emittance data, the solar absorption efficiency was calculated. Laser flash analysis, differential scanning calorimetry, and thermogravimetric analysis were utilized to determine thermal conductivity and specific heat. The solar absorptivity of the particles was initially measured at 0.90. After exposure to air at 1000 °C, it decreased to 0.73. However, following a reduction process, the particle recovered absorptivity of 0.90. The thermal aging and recovery were repeated multiple times, consistently achieving an absorptivity of 0.90. The thermal conductivity of the particles ranged from 0.50 to 0.88 W/(m-K). Solar absorptivity was found to be influenced by the types of iron oxide present in the particles. Particles with a predominance of hematite exhibited decreased solar absorptivity, while those containing magnetite, wüstite, and iron showed increased absorptivity. The estimated cost of the developed particles was more than ten times lower than that of current products. Given that component costs significantly impact the levelized cost of electricity (LCOE), this price reduction corresponded to an 8 % decrease in LCOE compared to other products. The low-cost thermal energy media show great promise for contributing to a reduced LCOE in the third generation of concentrating solar power systems.

1. Introduction

The generation 3 Concentrated Solar Power (Gen3 CSP) systems embody the latest breakthroughs in CSP technology, focusing on elevating efficiency, minimizing costs, and bolstering overall performance in solar energy generation [22,36]. As the renewable energy industry experiences rapid evolution, Gen3 CSP innovations leverage cutting-edge designs, advanced materials, and refined components to achieve exceptional solar-to-electric conversion efficiencies and optimize thermal energy storage capacities [21]. These pioneering technologies strive to reduce the environmental impact of solar energy production and offer versatile, modular configurations that accommodate an array of applications and geographical settings [21]. Although Gen3 CSP technologies have emerged more recently compared to their antecedents, their continuous development and maturation possess the capacity to substantially shape the solar energy sector and facilitate the establishment of a sustainable, low-carbon energy framework [37,11].

Gen3 CSP systems are gaining preference over their predecessors due to an array of benefits they offer. Gen3 CSP solutions employ sophisticated designs, materials, and components that lead to improved solar-to-electric conversion efficiencies, optimizing solar resource exploitation and amplifying electricity production [22]. These cutting-edge CSP technologies strive to lower the costs associated with solar power generation. By integrating cost-effective materials, components, and designs, Gen3 CSP systems reduce capital and operational expenses, making CSP a more competitive alternative among renewable energy sources [22]. Moreover, Gen3 CSP systems emphasize the incorporation of efficient and high-capacity Thermal Energy Storage (TES) solutions,

* Corresponding authors.
E-mail addresses: khan@advmatersci.com (K. Bum Han), Zhiwen.Ma@nrel.gov (Z. Ma).

https://doi.org/10.1016/j.solener.2024.112603
Received 26 July 2023; Received in revised form 17 October 2023; Accepted 6 May 2024

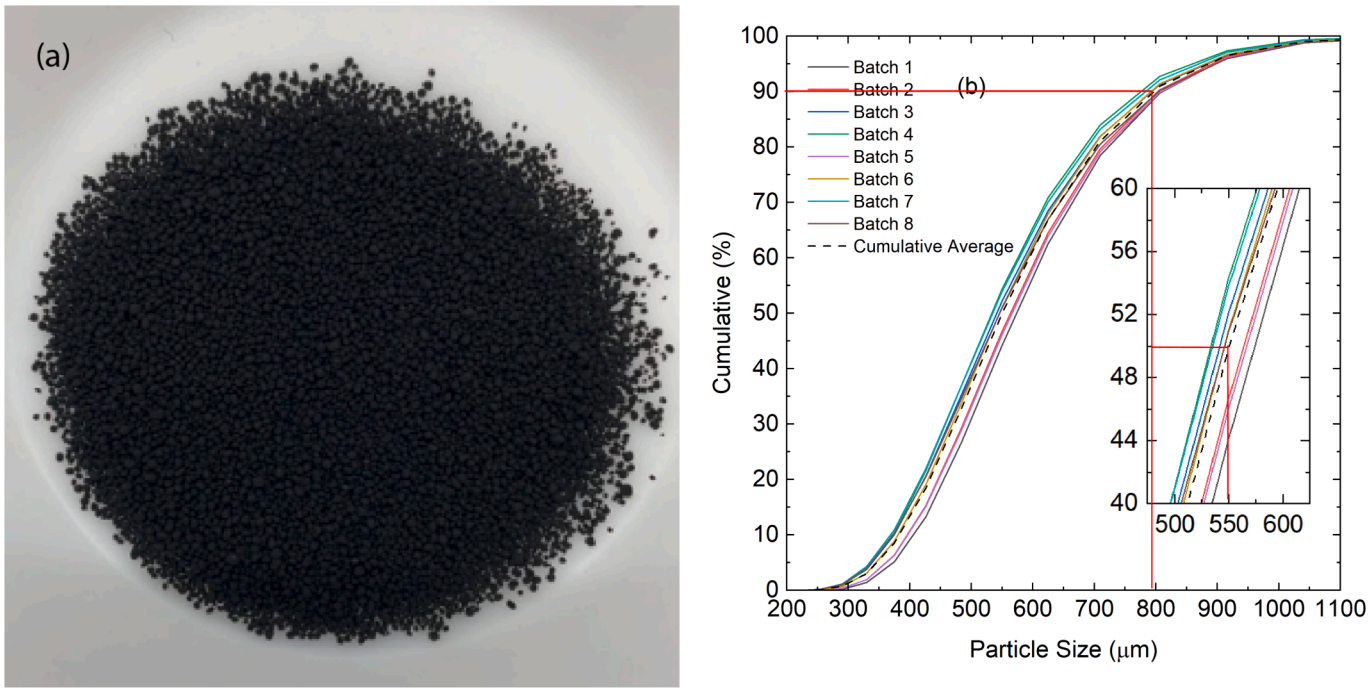

Fig. 1. (a) Visualization of black particles; and (b) particle size and distribution.

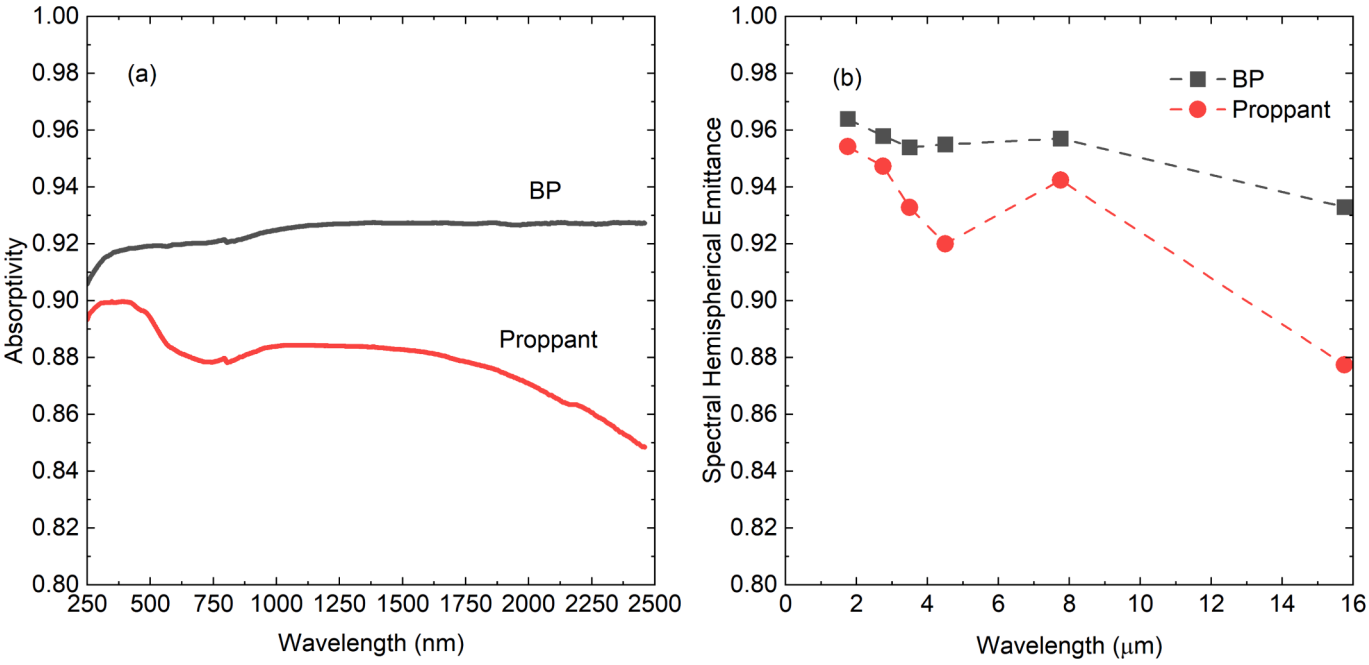

Fig. 2. (a) Absorptivity; and (b) spectral hemispherical emittance of black particles and ceramic proppant.

Table 1
Calculated absorber efficiency (η) utilizing the measured solar absorptivity (α) and emittance (ε).

Samples	α	ε	η
BP	0.92	0.93	0.84
Proppant	0.88	0.89	0.80

enabling CSP plants to store energy and deliver it on-demand [22]. This enhances the reliability and flexibility of electricity supply, especially during peak demand or periods of reduced solar radiation [22]. Furthermore, advanced CSP technologies aim to mitigate the environmental ramifications of solar power generation [22,37]. For instance, Gen3 CSP systems require less water for cooling, employ dry cooling techniques, and minimize the use of hazardous materials in their components, thus promoting the overall sustainability of the energy sector. Lastly, the scalability and modularity of Gen3 CSP technologies streamline installation, expansion, and maintenance procedures, increasing their appeal for a wide range of applications and locations [22]. This includes smaller-scale installations and distributed energy generation, further solidifying their position in the renewable energy landscapes.

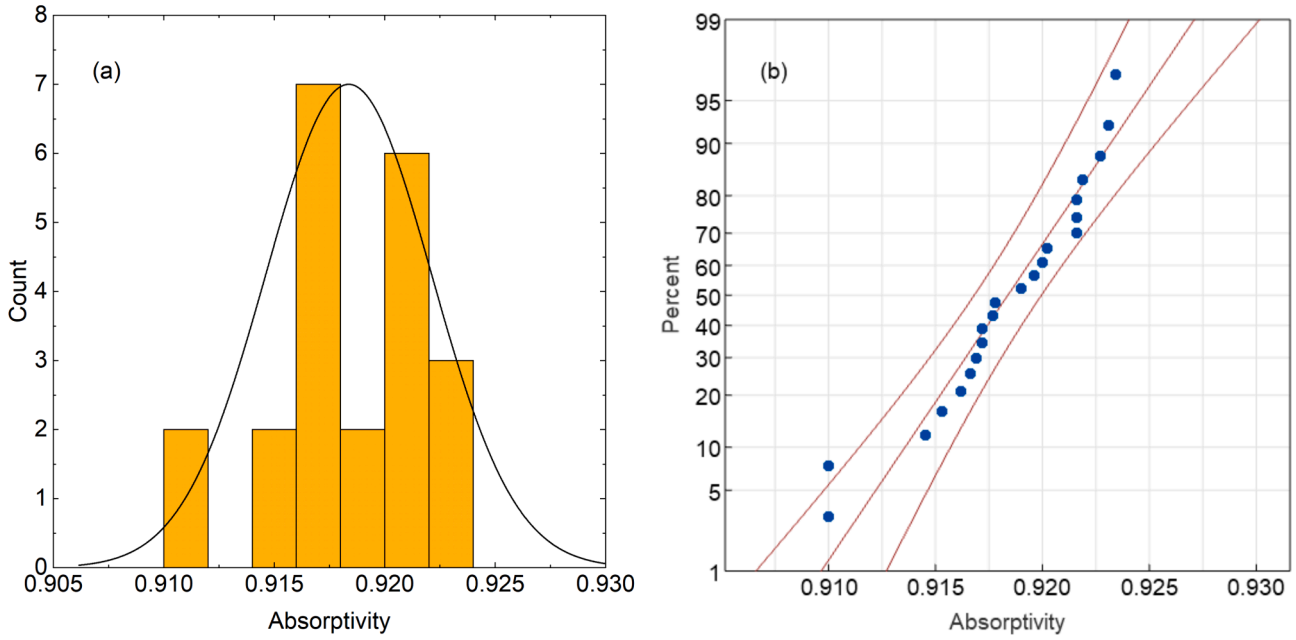

Fig. 3. (a) Distribution of absorptivity; and (b) probability plot for fabricated black particles.

Despite the superior performance attributes of Gen3 CSP systems, these technologies pose certain challenges in comparison to earlier generations. Primarily, the integration of advanced designs, materials, and components in Gen3 CSP systems heightens their complexity, potentially complicating manufacturing, installation, and maintenance procedures, and impacting overall system reliability [21]. The incorporation of metallic materials and components can lead to increased upfront investment costs when contrasted with earlier CSP systems [19]. Such metallic materials include nickel alloys, austenitic stainless steel, ferritic stainless steel, duplex steel, carbon steel, molybdenum, and cobalt. These materials have been demonstrated to operate effectively up to 750 °C [31].Owing to the relatively recent emergence of Gen3 CSP technologies, they may possess a limited operational history, leading to uncertainties regarding long-term performance, reliability, and durability. Furthermore, the CSP market has predominantly been characterized by earlier-generation technologies, and the established market presence of these systems could hinder the adoption and market penetration of nascent Gen3 CSP solutions. Nevertheless, despite these constraints, Gen3 CSP technologies have the potential to overcome numerous challenges encountered by earlier CSP generations. By increasing energy efficiency, lowering the levelized cost of electricity, decreasing installation and maintenance expenses, Gen3 CSP systems can become increasingly competitive and attractive for large-scale solar power generation [17]. Despite the presence of these challenges, a significant reduction in component costs could potentially resolve the majority of the issues.

In Gen3 CSP systems, particles serve a critical function in determining energy efficiency, heat transfer, energy storage, and cost-effectiveness [17,19,22,21,37]. The selection of particle material and its properties significantly influence the overall performance and feasibility of these systems for large-scale solar power generation. Certain particles, such as coal ash, are unsuitable for third-generation CSP due to their low particle density and heat capacity [17,20]. Additionally, particles employed in other industries have been utilized in research institutions, and coated particles have been investigated for CSP systems. However, these particles tend to be costly Siegel et al. [33], Siegel et al. [33], environmentally unfriendly [7,30], and involve complex processing [30]. Customized particles, offering both high performance and affordability, are vital for optimizing Gen3 CSP systems.

To meet the requirements of Gen3 CSP systems, engineered particles must possess four key advantages. First, particles act as solar energy absorbers, transforming solar energy into thermal energy when exposed to direct sunlight. The particle material and its optical properties significantly affect the system's efficiency in capturing and storing solar energy [17]. Second, particle heat transfer phenomena govern the transfer of thermal energy to a working fluid, such as gas or liquid [17]. This process is essential for generating steam or other high-temperature fluids that drive turbines to produce electricity. Particles with high thermal conductivity and specific heat capacity are preferred, as they facilitate efficient heat transfer to the working fluid. Third, particles function as a medium for thermal energy storage in CSP systems, a crucial advantage that allows for power generation even when sunlight is unavailable [17]. The thermal properties of particles, including their heat capacity and thermal stability, are critical factors in determining the efficiency and capacity of the energy storage system. Lastly, the choice of particles significantly impacts the overall cost of the CSP system [17,22]. Desirable particles are abundant, affordable, and environmentally friendly. Moreover, materials that can endure high temperatures and demonstrate minimal degradation over time help reduce the need for frequent replacements, thus lowering operational costs.

In this study, we performed an assessment of black particles, primarily focused on their optical properties, as their fundamental function is to capture sunlight. Furthermore, a comparative analysis was conducted to evaluate the cost of these particles, considering their thermal properties in comparison to alternative particles. The particle synthesis process remains undisclosed due to proprietary information.

2. Materials and methods

2.1. Particle size distribution

The black particle (BP) size distributions of eight distinct batches were characterized using Mie scattering with a Malvern Mastersizer 3000. Dry air dispersion and a refractive index of 2.420 (magnetite) were employed. To separate subsamples from the bulk sources and minimize the impact of particle segregation during transport, a particle sampling probe was utilized. Particle diameter data is presented in the D form (i.e., as the volume-weighted or mass moment mean) Standard [3], Standard [4].

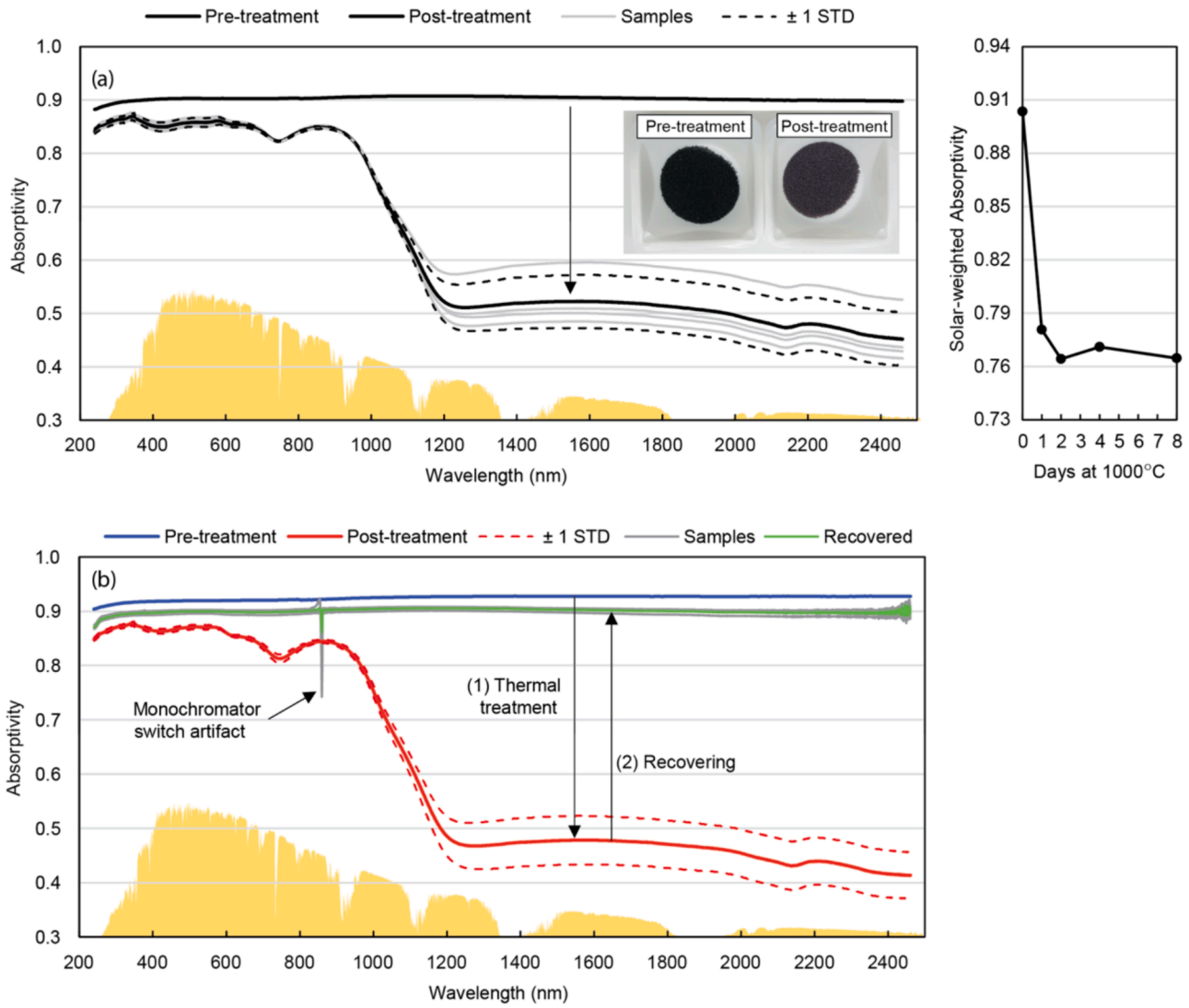

Fig. 4. (a) Absorptivity of pre-treated and post-treated black particles (BP) at 1000 °C in air; and (b) recovered absorptivity of post-treated BP.

2.2. Optical properties

The absorptivity is the most critical optical property examined in this study, as it determines the amount of energy absorbed by the particles. The spectral hemispherical reflectance of packed particle beds at room temperature was measured using a Perkin-Elmer Lambda 1050 UV–Vis-NIR spectrophotometer equipped with a 150 mm integrating sphere. Diffuse spectral reflectance data was gathered at 10 increments, ranging from 250 nm to 2500 nm. The spectral data was integrated over the AM1.5 solar spectrum for calculation purposes.

Thermal emittance was calculated from room temperature reflectance data obtained with a Surface Optics ET-100 Emissometer, measuring spectral reflectance over six discrete wavelength bands between 1500 nm and 21000 nm. The spectral emittance values were integrated over the spectral distribution of a black emitter at 700 °C [18]. Additionally, to demonstrate the reproducibility of absorptance, 22 separate BP samples were measured, and two different engineers produced BP on randomly selected dates. The collected data was statistically analyzed for stability, distribution, and normality. Minitab software was utilized for the statistical analysis.

The emittance spectrum can be influenced by temperature variations. Owing to the lack of equipment for real-time emittance measurements during temperature shifts, we extrapolated the emittance values obtained at ambient temperature to estimate those at 700 °C Siegel et al. [33], Siegel et al. [33], 2014). Emittance refers to the proportion of radiation a material emits relative to a black body at an identical temperature. The receiver tower captures this radiant heat, which is then used to heat a working fluid, subsequently generating electricity. The particles used within the receiver tower are designed to absorb the maximum amount of solar radiation, known as solar selective absorptance, to optimize heat absorption. Nevertheless, as these particles increase in temperature, they radiate a portion of their absorbed heat, especially in the infrared (IR) spectrum, termed as thermal emittance [2]. The IR spectrum is categorized as Near-IR (0.7 um – 1.4 um), Short-Wavelength IR (SWIR) (1.4 um – 3 um), Mid-Wavelength IR (MWIR) (3 um – 5 um), and Long-Wavelength IR (LWIR) (8 um – 12 um). Notably, while MWIR and LWIR emanate directly from objects, SWIR operates similarly to visible light, where photons are either reflected or absorbed by an object [8]. Given the objective to gauge the reflectivity of particles to sunlight photons, SWIR was chosen as the metric for emittance measurement.

2.3. Recoverability of optical properties

Four BP batches were utilized for thermal aging. Each batch contained 100 mL of BP. The batches were heated in air at 1000 °C with a heating rate of 10 °C/min from room temperature. Subsequently, the temperature was maintained for durations ranging from 1 day to 8 days.

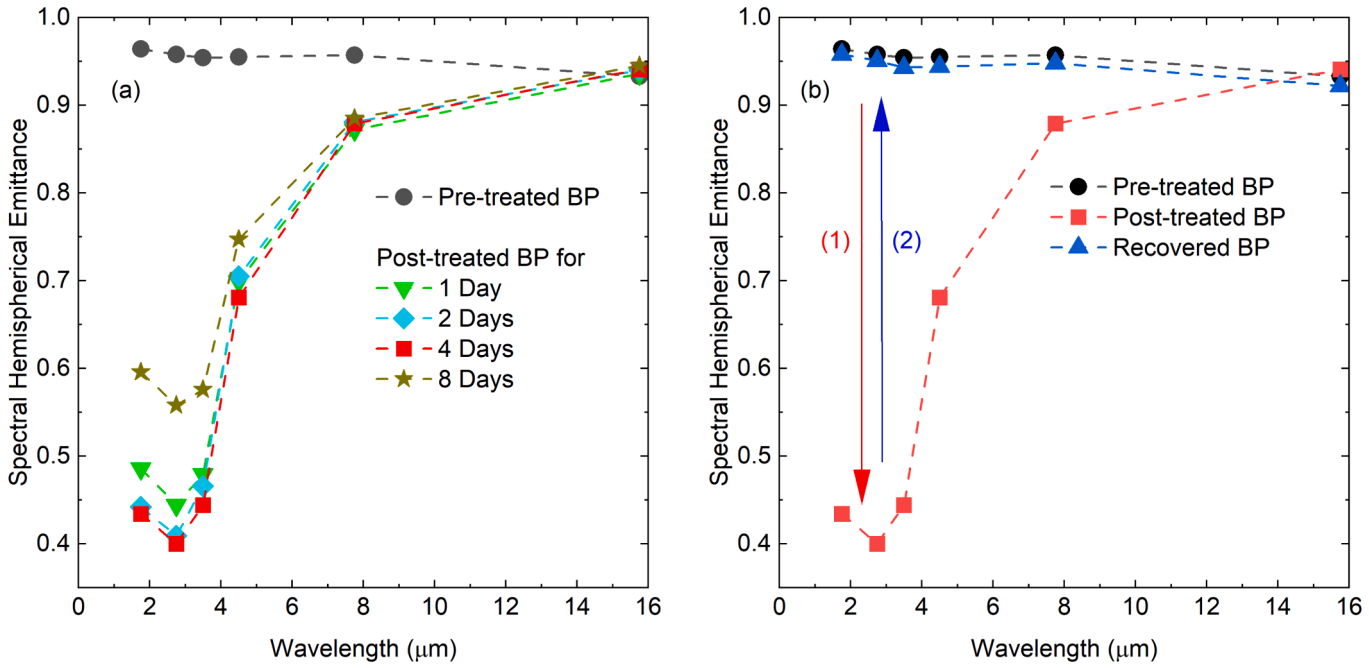

Fig. 5. (a) Spectral hemispherical emittance of pre-treated black particles (BP) and post-treated BP for various days at 1000 °C in air; and (b) recovered black particles via reduction at 400 °C.

Table 2
Absorber efficiency (η) of black particle (BP) batches subjected to exposure at 1000 °C in air and recovery at 400 °C via reduction.

	Pre-treated BP	Post-treated BP				Recovered BP
		1 Day	2 Days	4 Days	8 Days	
η	0.84	0.59	0.57	0.57	0.60	0.82

Other studies showed that the color of sintered bauxite proppants or thermal particles underwent a notable alternation when heated in air at temperatures exceeding 900 °C for a duration surpassing 150 h [14], Siegel et al. [33], Siegel et al. [33]. Consequently, for direct comparison to the previous studies, we chose a time frame extending to 8 days, beyond 150 h. After reaching the desired duration, the batches were allowed to cool down to room temperature naturally. The solar absorptance and thermal emittance were measured following the previously described method.

To determine the minimum duration required to restore the optical properties, the batches exposed to 1000 °C were reduced at 400 °C for varying durations. Additionally, recovery cycles were performed by exposing the samples in air at 1000 °C for 3 days and reducing them at 400 °C for 14 h under forming gas (5 % hydrogen balanced with argon).

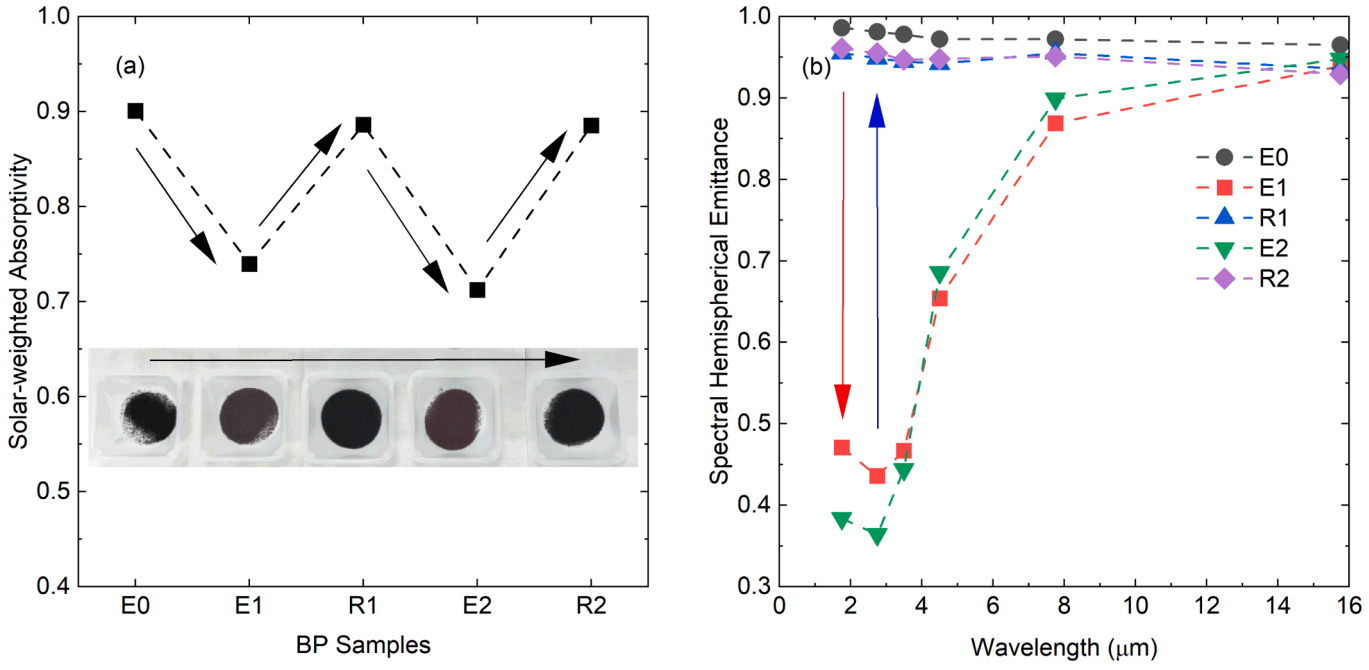

Fig. 6. (a) Solar-weighted absorptivity; and (b) spectral hemispherical emittance of black particles (BP) subjected to thermal cycles.

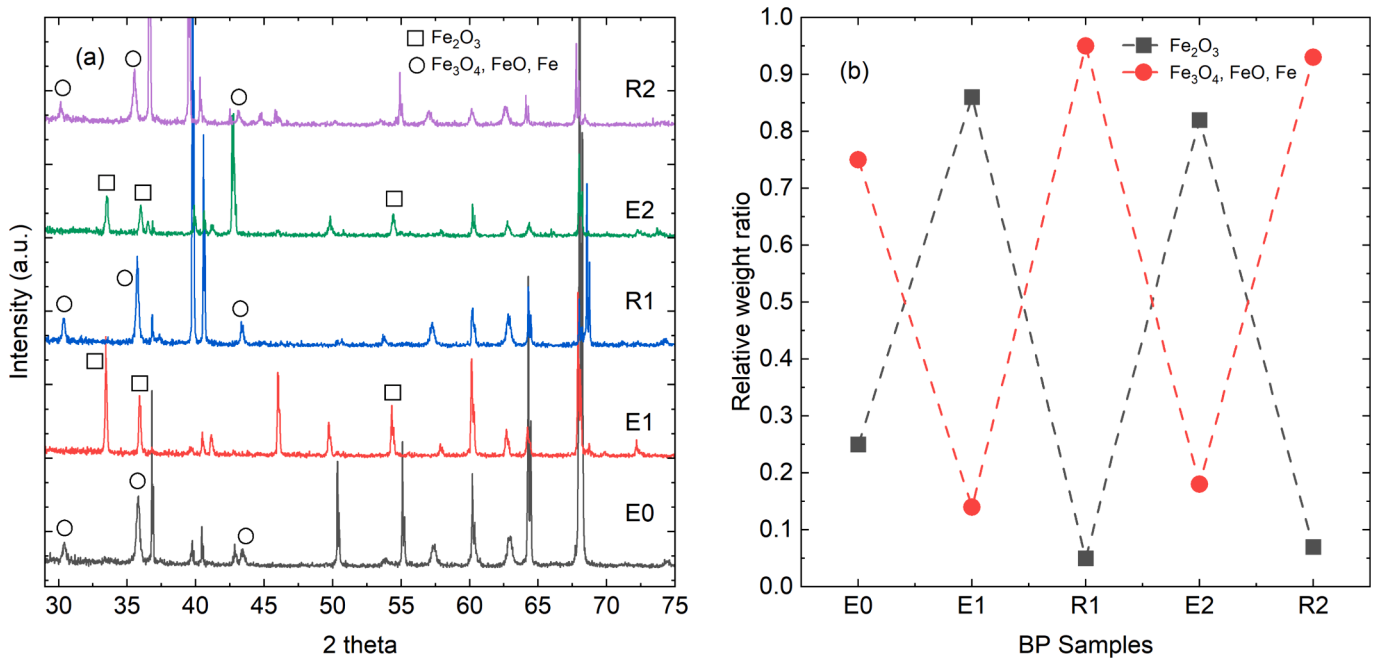

Fig. 7. (a) X-ray diffraction of black particles (BP) recovered multiple times; and (b) relative weight ratio between hematite and other iron oxides (magnetite, ferrous oxide, and iron).

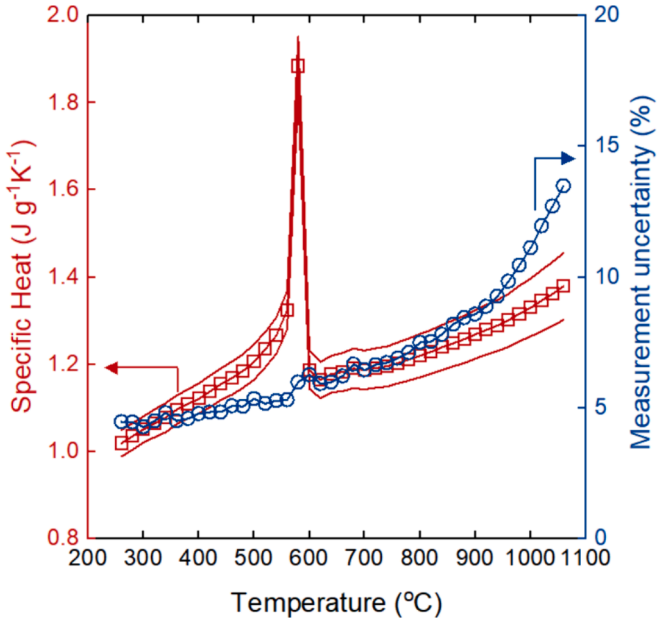

Fig. 8. Specific heat of black particles from 250 °C to 1050 °C.

The reduction duration was measured by empirical data presented S 1. The temperature of 400 °C was chosen to circumvent limitations arising from phase-boundary control. Pineau et al. demonstrated that the minimum temperature required to efficiently reduce iron oxide, while avoiding phase-boundary control limitations, is 400 °C [27]. Should reduction be dominated by phase-boundary control, the kinetics become slower, potentially leading to an ineffective reaction due to the deactivation of the reactant gas, namely hydrogen, when interacting with iron oxides [27]. This implies that the reduction process is not operating at optimal efficiency. For reasons of industrial safety and to ensure effective reduction, we have opted for this recommended temperature.

2.4. Thermal properties

The specific heat capacity as a function of temperature was measured using differential scanning calorimetry and thermogravimetric analysis (DSC/TGA) with an STA 449 F3 Jupiter instrument (Netzsch, Germany). A platinum crucible and lid were utilized during the measurement, and sapphire was used as a reference sample, measured three times. Three vacuum and purge cycles were carried out under the flow of ultra-high purity argon gas. The temperature range spanned from 25 °C to 1160 °C at a rate of 20 °C/min.

Thermal diffusivity was assessed via laser flash analysis (LFA 467 HT Hyperflash, Netzsch, Germany). A sapphire crucible and lid were employed in the measurement. The particles were loaded in the sapphire sample holder with inner diameter (12.5 mm) and height (3 mm). The holder was coated with graphite (S 2). The graphite coating promoted uniform heat absorption [5]. A xenon lamp flashes the samples when they have been heated to the desired temperature. On the opposite side of the sample, a liquid-nitrogen cooled infrared (IR) detector measures the temperature change that occurs over a set time. The laser flash analysis (LFA) showed partial transmittance through samples at high temperature (>800 °C)(S 3), resulting in poor fit. Thus, we limited the temperature to 800 °C. Eight samples were measured with three flashes per sample per temperature. The measurement was conducted in an ultra-high purity argon gas atmosphere under continuous flow at 120 mL/min. The temperature range extended from 25 °C to 800 °C with 20 °C increments. The uncertainty of the measured data is ± 10 %, based on the instrument calibration.

3. Results and discussion

3.1. Particle characterization

The black particle (BP) exhibited a notably dark color (Fig. 1(a)). The particle size distribution showed 410 μm at 10 %, 550 μm at 50 %, and 800 μm at 90 % (Fig. 1(b)), with an average size of 610 μm. Proppant CARBOHSP 40/70 (Carbo Ceramics, Inc., Houston, TX) was employed for comparison of absorptivity. The absorptivity of BP began above 0.90 and maintained intensity throughout the entire spectrum of interest

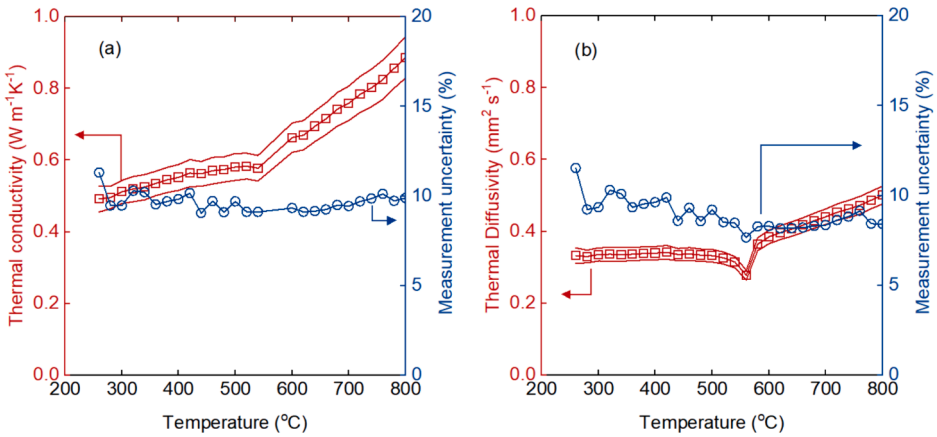

Fig. 9. (a) Thermal conductivity (b) thermal diffusivity from 260 °C to 800 °C.

Table 3
Summary of Thermal Media Properties, where α represents Solar Absorptivity; ε signifies Thermal Emittance; η denotes Calculated Absorber Efficiency; Cp refers Specific Heat; and k corresponds to Thermal Conductivity.

Thermal Media	Chemical Composition	Price (USD/ton)	α	η	Cp (J/(Kg·K))	k (W/(m·K))	Ref.
Coal Ash	SiO_2, Al_2O_3, Minerals	$10	0.5—0.7	0.43	949.7	0.46–0.52	[32,29]
Silica Sand	SiO_2	$30 – $40	<0.4	0.35	830	0.05–2.2	(Engineering [9,23]
Silicon Carbide	SiC	$50 – $70	0.9	0.83	750	120	[16]
Graphite	C	>$50	0.84	0.76	717	In-plane: 2000 Cross-plane:6.8	(Engineering [9,15]
Alumina	Al_2O_3	>$1,000	0.13	0.11	718	18	(Engineering [9,1]
Ceramic Proppant	Al_2O_3 (75 %) SiO_2 (11 %) Fe_2O_3 (9 %) TiO_2 (3 %)	$1,000-$2,000	0.87 (measured)	0.83 (measured)	1160	0.25–0.55	(Siegel et al., 2015a)
BP	Proprietary Information	$80 (calculated)	0.92 (measured)	0.87 (measured)	850–1250 (measured)	0.5–0.88 (measured)	This study

(Fig. 2(a)). Conversely, the proppant demonstrated diminished absorptivity with increasing wavelength.

The broader range of absorptive wavelengths affords better conversion efficiency of sunlight to electrical energy [24]. High absorptivity across a wide range of wavelengths enhances solar energy collection by allowing particles to absorb more sunlight and convert it into other forms of energy, such as heat or electricity, ultimately improving the efficiency and effectiveness of CSP systems. Additionally, high absorptivity minimizes optical losses in CSP systems caused by sunlight reflection or scattering, increasing the system's overall efficiency. Thirdly, the cloud, for example, can reduce available solar resource, but particles with high absorptivity in a broad range of wavelength perform better under varying weather conditions effectively absorbing solar energy even when sunlight intensity is reduced or the wavelength composition changes. Moreover, particles with high absorptivity tend to have advantageous thermal properties, efficiently absorbing and retaining heat [28].

The emittance of BP exhibited higher intensity than the proppant across the entire wavelength (Fig. 2(b)). The proppant's emittance pattern was consistent with other studies Siegel et al. [33], Siegel et al. [33], 2014). When paired with high absorptivity, elevated emittance offers distinct advantages. High absorptivity ensures optimal solar energy capture, while heightened emittance facilitates effective thermal radiation release post-sunlight absorption. This synergy can significantly enhance the efficiency of CSP systems by optimizing the conversion of solar energy into heat. Nevertheless, in scenarios where prolonged heat retention within the absorber is desired, elevated emittance might induce undesirable heat dissipations, potentially diminishing efficiency. Thus, the implications of pronounced thermal emittance on absorber efficiency are intrinsically tied to specific applications and the nuances of system design. For CSP systems aiming for immediate heat utilization, a pronounced emittance proves advantageous. The absorptivity and thermal emittance data were utilized to determine the absorber efficiency (η) according to the following calculation [6]:

$$\eta = \frac{\alpha \bullet Q - \varepsilon \bullet \sigma \bullet T^4}{Q} \quad (1)$$

where α is the solar absorptivity, Q is assumed to be $6 \times 10^5 W/m^2$, ε is the thermal emittance, σ is the Stetan-Boltzmann constant $\left(5.67 \times 10^{-8} W/m^2K^4\right)$ [6], and T is an assumed surface temperature of 700 °C [6]. The average values from 8 samples were plotted in Fig. 2. The BP sample showed an absorber efficiency increase of 0.04 (4 %) over to the proppant (Table 1).

The absorptivity distribution of 22 fabricated BP batches, along with a normal curve, is illustrated in Fig. 3(a). The mean value was 0.9184, with a standard deviation of 0.0038. The minimum and maximum values were 0.9100 and 0.9234, respectively, and the median was 0.9184. The absorptivity data at 0.910 slightly exceeded the distribution curve. Fig. 3(b) displays the probability plot assessing the fit of a distribution to the data. The Anderson-Darling (AD) statistic method was employed for the normality test, yielding a p-value of 0.206 and an AD value of 0.484. Most data points aligned with the fitted distribution line, except for one data point at 0.910. Consequently, the BP absorptivity was approximately 0.92.

3.2. *Thermal aging and recovery optical properties*

A thermal aging test was performed to evaluate changes in solar absorptivity at elevated temperatures. Four separate batches were

elevated to a high temperature of 1000 °C for durations ranging from 1 to 8 days. The graphs from Fig. 4 show both the average of 8 batches and all 8 samples. The solid lines are the average with darker color. The solid lines with a lighter color are spectra from individual 8 samples. All batches exhibited a decrease in absorptivity: a significant decline was observed between 1200 nm and 2500 nm, while a slight decrease was noted in the visible wavelengths, as illustrated in Fig. 4(a). Following a 4-day exposure to 1000 °C in an air atmosphere, the color of the black particles (BP) (Pre-treatment) transitioned to dark gray (Post-treatment). The post-treated BP was selected for recovering the absorptivity. Upon subjecting the exposed BP batches to a reduction reaction with forming gas, comprising 5 % hydrogen and 95 % argon, absorptivity was nearly restored to its initial intensity, as depicted in Fig. 4 (b). The spectral hemispherical emittance of BPs dropped from 1.75 μm to 7.75 μm (Fig. 5(a)) after exposure at 1000 °C in air from 1 day to 8 days. It was unknown the sample at 8 Days showed higher emittance and other pre-treated BP for days. The emittance was restored to its original intensity following the reduction in the entire wavelength (Fig. 5(b)). Table 2 presents the calculated absorber efficiency of the pre-treated, post-treated, and recovered BPs. Efficiency dropped from 0.84 to a range of 0.57–0.60 after exposure to high temperatures in air for various days. However, following the reduction, the efficiency was recovered to 0.82.

Several advantages arise from recoverability of optical properties. Particles that regain high absorptivity can efficiently absorb sunlight once again. In addition, recoverability leads to improved energy conversion rates, translating to higher overall system efficiency. This indicates more electricity generated per unit of solar radiation, consequently reducing the levelized cost of electricity. Third, CSP systems can maintain consistent performance levels and operate more reliably, reducing the risk of underperformance or system failure. Fourth, recoverable particles can continue to perform their intended function, extending the lifespan of the solar receiver and supporting components in CSP systems. This results in lower maintenance costs and a longer overall system life. Moreover, recovery helps maintain the system's performance without the need for replacing components, reducing costs associated with repairs or replacements. Lastly, the environmental benefit is notable. Enhanced performance due to regained high absorptivity contributes to higher energy production from renewable sources, reducing reliance on fossil fuels and lowering greenhouse gas emissions.

3.3. Recovering optical properties by thermal cycles

It was significant to understand that the recovery could be performed multiple times. The images and measured absorptivity of the batch are shown in Fig. 6(a). The BP particles (E0) demonstrated high absorptivity at 0.90. To recover the absorptivity, a post-treated BP batch (E1), exposed in air at 1000 °C for 3 days, was placed in the reduction at 400 °C for 3 h in forming gas (R1). Subsequently, the recovered batch was exposed in air at 1000 °C for 3 days (E2). The second exposure was recovered under the same reduction conditions (R2). Qualitatively, the particle color became lighter or gray color after exposure, but the color was restored to dark after reduction. The absorptivity was recovered to near 0.90 multiple times, even though the batch lost absorptivity to 0.70 – 0.75 after exposure. The emittance of the exposed and recovered BP from 1.75 μm to 16.7 μm is depicted in Fig. 6(b). The emittance exhibited the same trend as the absorptivity. The exposed BP decreased the emittance, which was recovered after reduction.

The crystal structure of the exposed and recovered particles was characterized using X-ray diffraction (XRD), as shown in Fig. 7(a). The exposed BP particles (E0) primarily exhibited hematite. However, after recovery, most iron oxides were identified as magnetite (Fe_3O_4), wüstite (FeO), and iron (Fe). When the recovered particles were exposed in air at 1000 °C, the iron oxide structure transitioned to hematite, as depicted in Fig. 7(b). The reduction subsequently recovered magnetite, wüstite, and iron. Consequently, high absorptivity was recovered by converting hematite to other types of iron oxide because hematite has relatively lower absorptivity. For instance, hematite has 0.87 absorptivity [26] while magnetite was 0.95–0.97 [35].

3.4. Thermal properties

The specific heat capacity represents the amount of heat required to raise the temperature of one unit mass of particles by one unit. The specific heat capacity of BP began at 0.9 J/g·K at 250 °C and increased to 1.25 J/g·K at 800 °C, as illustrated in Fig. 8. The results indicated a phase change near 580 °C signifying the phase change of magnetite [12,13].

Fig. 9(a) and (b) displays the thermal conductivity and diffusivity of BP, which is one of the essential thermal properties for media used in thermal energy storage (TES) systems. Higher thermal conductivity in particles facilitates faster heat loading or releasing rates within the TES system. Thermal diffusivity showed a phase transition at 580 °C. The diffusivity peak at 580 °C implied magnetite corresponded to hematite as increasing the temperature [13,25]. Grosu, Y. et al. indicated the peak to reversible phase transition [13]. The stored/released energy obtained by the endothermic/exothermic enthalpy of the reversible transformation could be beneficial in the thermal energy storage field [13].

Table 3 summarizes the current media for Gen3 CSP systems. Among the materials listed, Black Particle (BP) stands out with its impressive properties. It exhibits the highest absorptivity and emittance, and its specific heat is comparable to that of the ceramic proppant. Furthermore, BP has a higher thermal conductivity compared to the ceramic proppant. The thermal conductivity of ceramic proppant is similar to that of phase change materials (PCMs), such as polyethylene, which has a thermal conductivity of 0.3–0.5 W/(m•K) [38]. Polyethylene is a material commonly used in thermal energy storage for CSP systems. The superior thermal properties of BP allow for more efficient heat transfer between the media and the heat transfer fluid (HTF) used in CSP systems. This efficient heat transfer results in faster charging and discharging times for the storage system, ultimately enhancing the overall efficiency of the system. Gen3 CSP systems aim to achieve a higher level of efficiency compared to older systems. With its increased thermal conductivity, BP aids in effective heat transfer between the solar-absorbing surface and the working fluid. This leads to elevated temperatures and minimal heat losses. As a result, Black Particle (BP) emerges as a top-performing material in CSP systems, delivering unparalleled system efficiency due to its high thermal conductivity.

As per Table 3, even though we divulge specific details about the composition and fabrication process of BP due to proprietary constraints, the comprehensive cost of BP, which includes overhead and all other sales-related expenses, is estimated at 80 USD per ton, while the ceramic proppant's cost is 1,000 USD per ton or higher. The BP's projected Levelized Cost of Energy (LCOE) is approximately 0.060 USD/kWh, whereas the ceramic proppant's LCOE stands at 0.065 USD/kWh or above. This represents an 8 % reduction in cost when utilizing BP compared to ceramic proppant.

Achieving a low cost of particles is considered critical to reduce the levelized cost of electricity (LCOE) in Gen3 CSP systems. LCOE represents the average cost per unit of electricity generated over the lifetime of a power plant, accounting for all the costs involved, such as capital, operations and maintenance, and fuel costs. To make CSP more competitive with other energy sources, it is essential to minimize LCOE. The cost of particles used in the system has a direct impact on the LCOE. Particles, as heat transfer media and thermal energy storage materials, constitute a significant portion of the material costs in GEN3 CSP systems. Reducing the cost of particles can contribute to lower initial capital investment and overall material costs, leading to a decrease in LCOE. This is because the particle cost contributes 10 % for the optimal CSP plant configuration [10]. Moreover, the particle cost is the second most impactful parameter on LCOE with 25 % of uncertainty [10]. The

particle cost has the greatest impact on LCOE for the case with 50 % of uncertainty [10]. Lower-cost particles allow for the use of larger quantities or higher-performance materials without substantially increasing the overall cost. This can potentially improve the efficiency of heat transfer, energy storage, and energy conversion processes, which in turn can lower the LCOE. Achieving a lower cost per ton of particles can facilitate the deployment of larger CSP plants, taking advantage of economies of scale to further reduce LCOE. Larger plants can typically achieve lower costs per unit of electricity generated due to more efficient utilization of resources and infrastructure. Reducing the LCOE is vital for the competitiveness of CSP systems compared to alternative energy sources, such as solar photovoltaic, wind, or natural gas. Achieving a lower cost for particles helps decrease the LCOE.

The LCOE model showed there was a positive correlation between receiver efficiency and the increase in solar weighted absorptance [34]. However, as particles lost their absorptance over time due to oxidation, the efficiency correspondingly diminished. Restoring the particles' high absorptance through reduction ensures that the particle receiver maintains its peak efficiency. The Levelized Cost of Electricity (LCOE) calculations in this study focused solely on the optical properties of the particles. For instance, in these LCOE calculations, we have presupposed that particles consistently retain a high absorptivity of approximately 0.9, without accounting for other variables related to the reduction process. Future research on LCOE will require a more comprehensive evaluation, encompassing all intricacies associated with the reduction procedure.

4. Conclusion

In this study, we investigated the optical properties of black particles (BP) to assess their potential as thermal energy media in generation 3 Concentrated Solar Power (Gen3 CSP) systems. Gen3 CSP offers several advantages over previous-generation systems, including higher efficiency, lower costs, enhanced thermal energy storage, modular design, reduced water usage, environmental benefits, and improved reliability and durability. To fully capitalize on Gen3 CSP's potential, it is crucial to develop and incorporate suitable components tailored to its advanced capabilities.

Particles serve as a vital component in Gen3 CSP systems, playing a critical role in their performance. While current particles in use and under research demonstrate remarkable absorption properties, challenges persist, such as high costs that prevent the Levelized Cost of Energy (LCOE) from falling below 0.05 USD/kWh. When lower-cost alternatives are utilized, they often exhibit compromised absorption capabilities, leading to reduced energy efficiency. Moreover, some particles are made of materials that pose significant environmental concerns due to pollution.

The black particles displayed exceptional optical properties and an extremely low cost. Although absorptivity decreased during the thermal aging test, the black particles demonstrated their potential for recovery of optical properties. Addressing these limitations remains a primary focus for AMS in their ongoing development efforts.

In conclusion, the black particles hold the potential to play a crucial role in helping Gen3 CSP systems achieve the targeted low LCOE. Their importance in advancing this technology is evident, and continued research and development of these particles will contribute significantly to the progress of Gen3 CSP systems in the renewable energy landscape.

Declaration of Competing Interest

The authors declare that they have no known competing financial interests or personal relationships that could have appeared to influence the work reported in this paper.

Acknowledgements

This study is based upon work supported by the U.S. Department of Energy (Office of Science and Solar Energy Technologies Office), Washington Clean Energy Testbeds at University of Washington, and Materials Characterization Laboratory at University of Utah under Award Number DE-SC00021751.

Appendix A. Supplementary data

Supplementary data to this article can be found online at https://doi.org/10.1016/j.solener.2024.112603.

References

[1] Accuratus, 2013. Aluminum oxide material properties. URL https://accuratus.com/alumox.html (accessed 12.22.22).
[2] Ambrosini, A., Lambert, T.N., Bencomo, M., Hall, A., vanEvery, K., Siegel, N.P., Ho, C.K., 2011. Improved High Temperature Solar Absorbers for Use in Concentrating Solar Power Central Receiver Applications, in: ES2011. ASME 2011 5th International Conference on Energy Sustainability, Parts A, B, and C, pp. 587–594.
[3] ASTM Standard, 2012a. Standard test method for solar absorptance, reflectance, and transmittance of materials using integrating spheres (No. ASTM E903-12). American National Standards Institute, West Conshohocken, PA.
[4] ASTM Standard, 2012b. Standard tables for reference solar spectral irradiances: direct normal and hemispherical on 37° tilted surface (No. ASTM G173-03). American National Standards Institute, West Conshohocken, PA.
[5] Brankovic, S.A., Arkhurst, B., Gunawan, A., Yee, S.K., 2020. High-Temperature Thermophysical Property Measurement of Proposed Gen3 CSP Containment Materials, in: ES2020. ASME 2020 14th International Conference on Energy Sustainability. https://doi.org/10.1115/ES2020-1687.
[6] A. Calderón, C. Barreneche, A. Palacios, M. Segarra, C. Prieto, A. Rodriguez-Sanchez, A. Fernández, Review of solid particle materials for heat transfer fluid and thermal energy storage in solar thermal power plants, Energy Storage 1 (2019) e63.
[7] K. Chung, R. Chen, Black coating of quartz sand towards low-cost solar-absorbing and thermal energy storage material for concentrating solar power, Sol. Energy 249 (2023) 98–106.
[8] E. Optics What is SWIR? | Edmund Optics [WWW Document] https://www.edmundoptics.com/knowledge-center/application-notes/imaging/what-is-swir/ 2023 accessed 10.15.23.
[9] E. ToolBox Specific heat of common substances https://www.engineeringtoolbox.com/specific-heat-capacity-d_391.html 2003 accessed 12.22.22.
[10] L. González-Portillo, K. Albrecht, J. Sment, B. Mills, C. Ho, Sensitivity analysis of the levelized cost of electricity for a particle-based concentrating solar power system, J. Sol. Energy Eng. 144 (2022) 030902–030910.
[11] J. Greenblatt, N. Brown, R. Slaybaugh, T. Wilks, E. Stewart, S. McCoy, The future of low-carbon electricity, Annu. Rev. Environ. Resour. 42 (2017) 289–316.
[12] F. Grønvold, A. Sveen, Heat capacity and thermodynamic properties of synthetic magnetite (Fe 3O 4) from 300 to 1050 K. Ferrimagnetic transition and zero-point entropy, J. Chem. Thermodyn. 6 (1974) 859–872, https://doi.org/10.1016/0021-9614(74)90230-4.
[13] Y. Grosu, A. Faik, I. Ortega-Fernández, B. D'Aguanno, Natural Magnetite for thermal energy storage: Excellent thermophysical properties, reversible latent heat transition and controlled thermal conductivity, Sol. Energy Mater. Sol. Cells 161 (2017) 170–176, https://doi.org/10.1016/j.solmat.2016.12.006.
[14] Hellmann, J.R., Eatough, M.O., Hlava, P.F., Mahoney, A.R., 1987. Evaluation of Spherical Ceramic Particles for Solar Thermal Transfer Media (No. SAND86- 0981). Sandia National Laboratory, Albuquerque, NM.
[15] K. Hippalgaonkar J. Hun Seol D. Xu D. Li Chapter 12 - Experimental Studies of Thermal Transport in Nanostructures G. Zhang Thermal Transport in Carbon-Based Nanomaterials 2017 Elsevier Micro and Nano Technologies 319 357.
[16] IMetra, 2023. Silicon carbide material properties. Imetra Inc. URL https://www.imetra.com/silicon-carbide-material-properties/ (accessed 12.22.22).
[17] M. Imran Khan, F. Asfand, S. Al-Ghamdi, Progress in technology advancements for next generation concentrated solar power using solid particle receivers, Sustain. Energy Technol. Assess. 54 (2022) 102813.
[18] F. Incropera, D. DeWitt, Introduction to Heat Transfer, third. ed., Wiley, New York, 1996.
[19] Kraemer, S., 2018. What are the pros and cons of longer solar contracts? SolarPACES. URL https://www.solarpaces.org/what-are-the-pros-and-cons-of-longer-solar-contracts/ (accessed 4.5.23).
[20] Ma, Z., Zhang, R., Sawaged, F., 2017. Design of particle-based thermal energy storage for a concentrating solar power system, in: ES2017. Presented at the ASME 2017 11th International Conference on Energy Sustainability, ASME, Charlotte, NC.
[21] Mehos, M., Turchi, C., Jorgenson, J., Paul, D., Ho, C., Armijo, K., 2016. On the path to SunShot: advancing concentrating solar power technology, performance, and dispatchability (No. NREL/TP-5500-65688). NREL, Golden, CO.
[22] Mehos, M., Turchi, C., Vidal, J., Wagner, M., Ma, Z., Ho, C., Kolb, W., Andraka, C., Kruizenga, A., 2017. Concentrating solar power Gen3 demonstration roadmap (No. NREL/TP-5500-67464). NREL, Golden, CO.

[23] K. Midttømme, E. Roaldset, The effect of grain size on thermal conductivity of quartz sands and silts, Pet. Geosci. 4 (1998) 165–172.
[24] Nayfeh, M. (Ed.), 2018. Chapter 13 - Advanced and Low Cost Energy and Lighting Devices, in: Fundamentals and Applications of Nano Silicon in Plasmonics and Fullerines, Micro and Nano Technologies. Elsevier, pp. 363–429.
[25] Noda, Y., Naito, K., 1978. The Thermal Conductivity and Diffusivity of Mnx Fe3-xO4 (0≦x≦1.5) from 200 to 700K. NETSU 5.
[26] A. Palacios, A. Calderón, C. Barreneche, J. Bertomeu, M. Segarra, A.I. Fernández, Study on solar absorptance and thermal stability of solid particles materials used as TES at high temperature on different aging stages for CSP applications, Sol. Energy Mater. Sol. Cells 201 (2019) 110088.
[27] A. Pineau, N. Kanari, I. Gaballah, Kinetics of reduction of iron oxides by H2: Part II. Low temperature reduction of magnetite, Thermochim. Acta 456 (2007) 75–88.
[28] T. Rasheed, T. Hussain, M. Anwar, J. Ali, K. Rizwan, M. Bilal, F. Alshammari, N. Alwadai, A. Almuslem, Hybrid nanofluids as renewable and sustainable colloidal suspensions for potential photovoltaic/thermal and solar energy applications, Front. Chem. 9 (2021) 1–20.
[29] H. Rezaei, R. Gupta, G. Bryant, J. Hart, G.S. Liu, C. Bailey, T. Wall, S. Miyamae, K. Makino, Y. Endo, Thermal conductivity of coal ash and slags and models used, Fuel 79 (2000) 1697–1710.
[30] E. Rubin, Y. Chen, R. Chen, Optical properties and thermal stability of Cu spinel oxide nanoparticle solar absorber coatings, Sol. Energy Mater. Sol. Cells 195 (2019) 81–88.
[31] M. Sarvghad, S. Delkasar Maher, D. Collard, M. Tassan, G. Will, T.A. Steinberg, Materials compatibility for the next generation of Concentrated Solar Power plants, Energy Storage Mater. 14 (2018) 179–198.
[32] P. Shetty, V. Atgur, P. Naik, Experimental evaluation of specific heat carrying capacity of fly-ash reinforced aluminium 6061 composite, IRJET 2 (2016) 774–780.
[33] N. Siegel, M. Gross, R. Coury, The development of direct absorption and storage media for falling particle solar central receivers, J. Sol. Energy Eng. 137 (2015) 1–7.
[34] N. Siegel, M. Gross, C. Ho, T. Phan, J. Yuan, Physical properties of solid particle thermal energy storage media for concentrating solar power applications, Energy Procedia 49 (2014) 1015–1023.
[35] V. Strapolova, E. Yurtov, A. Muradova, A. Sharapaev, Effect of magnetite nanoparticles' modification on optical properties of solar absorber coatings, J. Spacecr. Rockets 55 (2018) 49–53.
[36] Turchi, C., 2023. Generation 3 concentrating solar power systems. Conc. Sol. Power. URL https://www.nrel.gov/csp/generation-3-concentrating-solar-power-systems.html (accessed 4.5.23).
[37] World Bank, Concentrating Solar Power: Clean Power on Demand 24/7, World Bank, Washington DC, 2021.
[38] C. Yang, M. Navarro, B. Zhao, G. Leng, G. Xu, L. Wang, Y. Jin, Y. Ding, Thermal conductivity enhancement of recycled high density polyethylene as a storage media for latent heat thermal energy storage, Sol. Energy Mater. Sol. Cells 152 (2016) 103–110.